Los Alamos
NATIONAL LABORATORY
EST. 1943

LA-UR-16-24352
Approved for public release; distribution is unlimited.

Title: Verification Test of the SURF and SURFplus Models in xRage: Part II

Author(s): Menikoff, Ralph

Intended for: Report

Issued: 2016-06-20

Disclaimer:
Los Alamos National Laboratory, an affirmative action/equal opportunity employer, is operated by the Los Alamos National Security, LLC for the National Nuclear Security Administration of the U.S. Department of Energy under contract DE-AC52-06NA25396. By approving this article, the publisher recognizes that the U.S. Government retains nonexclusive, royalty-free license to publish or reproduce the published form of this contribution, or to allow others to do so, for U.S. Government purposes. Los Alamos National Laboratory requests that the publisher identify this article as work performed under the auspices of the U.S. Department of Energy. Los Alamos National Laboratory strongly supports academic freedom and a researcher's right to publish; as an institution, however, the Laboratory does not endorse the viewpoint of a publication or guarantee its technical correctness.

Verification test of the SURF and SURFplus models in xRage: Part II

Ralph Menikoff

June 20, 2016

Abstract

The previous study used an underdriven detonation wave (steady ZND reaction zone profile followed by a scale invariant rarefaction wave) for PBX 9502 as a validation test of the implementation of the SURF and SURFplus models in the `xRage` code. Even with a fairly fine uniform mesh (12,800 cells for 100 mm) the detonation wave profile had limited resolution due to the thin reaction zone width (0.18 mm) for the fast SURF burn rate. Here we study the effect of finer resolution by comparing results of simulations with cell sizes of 8, 2 and 1 μm, which corresponds to 25, 100 and 200 points within the reaction zone. With finer resolution the lead shock pressure is closer to the von Neumann spike pressure, and there is less noise in the rarefaction wave due to fluctuations within the reaction zone. As a result the average error decreases. The pointwise error is still dominated by the smearing the pressure kink in the vicinity of the sonic point which occurs at the end of the reaction zone.

1 Introduction

The previous study [Menikoff, 2016] used an underdriven detonation wave for PBX 9502 as a validation test of the implementation of the SURF and SURFplus models [Shaw and Menikoff, 2010, Menikoff and Shaw, 2010, 2012] in the `xRage` code. The exact solution for the SURF model is shown in fig. 1 at the start and end of the simulations. The simulation ends after $10\,\mu$s, and corresponds to propagating the detonation wave for about 80 mm. The solution is composed of a steady ZND reaction zone followed by a rarefaction (known as a Taylor wave) which spreads out in time and then a constant state to match the left boundary condition of a rigid wall; see for example ref. [Fickett and Davis, 1979, § 2C].

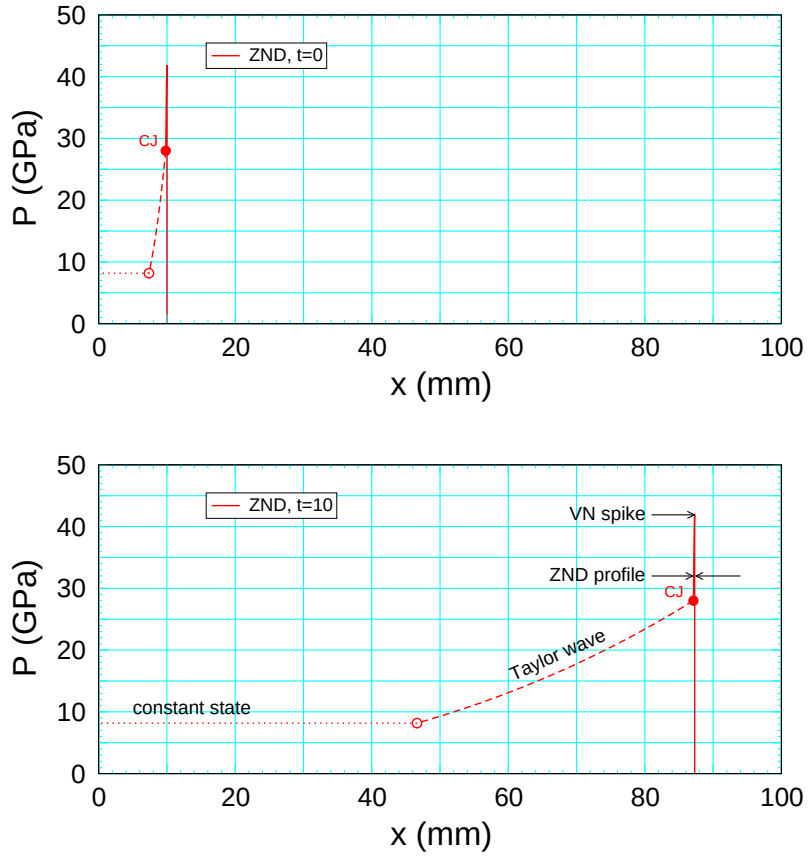

Figure 1: Exact pressure profiles at the start ($t = 0$) and end ($t = 10\,\mu$s) for simulations with the SURF model. Solid curve is ZND reaction zone. Dashed curve is Taylor wave, and dotted line is constant state. Solid and open circles are the head and tail of the Taylor wave.

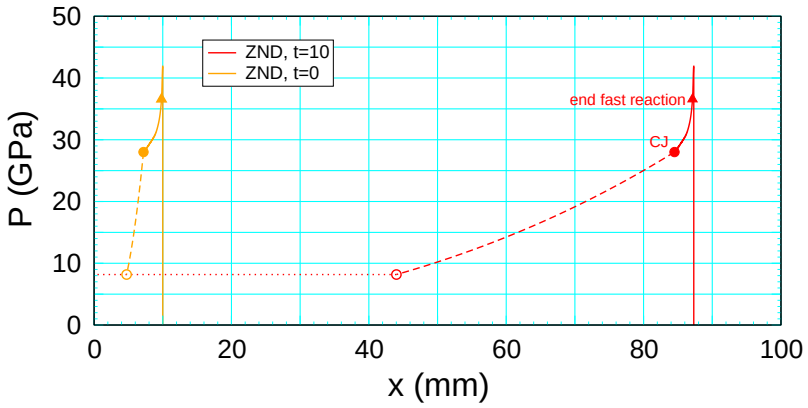

Figure 2: Exact pressure profiles at the start ($t = 0$) and end ($t = 10\,\mu$s) for simulations with the SURFplus model. Solid curves are ZND reaction zone. Dashed curves are Taylor wave, and dotted line is constant state.

The SURFplus model adds a second slow reaction for the energy release from carbon clustering. The exact solution is shown in fig. 2. The detonation wave with the SURFplus model has the same CJ- and VN-spike states as the SURF model. The models also used the same SURF parameters for the fast burn rate. However, for the SURFplus model, the SURF reaction ends with a higher pressure since the carbon clustering energy is released later. Due to the wider reaction zone from the slow rate, the pressure derivative at the CJ state is smaller for SURFplus than for SURF. Consequently, at the end of the simulation, the kink in the pressure profile (discontinuity in derivative) at the end of the reaction zone (CJ state) is smaller in magnitude for the SURFplus model.

The previous study focused on simulations utilizing a fairly fine uniform mesh (12,800 cells for 100 mm). Due to the thin reaction zone width, 0.18 mm, the resolution of wave profile for the fast SURF reaction was limited. Here we study the effect of finer resolution by comparing results of simulations with 128, 512, 1024 cells per mm; *i.e.*, 1, 4 and 8 times finer than previous study. This corresponds to roughly 25, 100 and 200 points within the SURF reaction zone for cell sizes of 8, 2 and 1 μm, respectively.

We focus on the pressure profile. For each simulation results will be presented for the pointwise error; difference of the pressure for the simulated and exact solutions. As an overall metric we use $\|P - P_e\|/P_{\rm CJ}$ where $P_{\rm CJ}$ is the detonation pressure and

$$\|P - P_e\|^2 = \frac{\sum_{i=1}^{N-1} \left(\frac{1}{2}\Big[P_i + P_{i+1}\Big] - \frac{1}{2}\Big[P_e(x_i - \Delta x, t) + P_e(x_{i+1} - \Delta x, t)\Big] \right)^2 \Big(x_{i+1} - x_i\Big)}{x_N - x_1} \,, \quad (1)$$

is a numerical approximation of the L_2-norm of the pressure difference. Here P_i is the numerical solution at the center of the i^{th} cell at time t, and $P_e(x_i - \Delta x, t)$ is the corresponding exact solution. To exclude the error from the numerical shock profile, N is taken such that P_N is the maximum pressure; *i.e.*, x_N corresponds to the shock front.

The exact solution is shifted in space by Δx such that the average of the pressure difference is 0. This enables the smeared out numerical shock front to be aligned with the discontinuous shock front of the exact solution. Since the numerical shock profile is a fixed number of cells, Δx decreases with finer resolution. For very fine resolution, Δx has a small effect on the metric. However, due to the large slope of the pressure profile, even a small shift affects the pointwise error within the reaction zone.

An unusual aspect of the SURF model is that the burn rate depends on the lead shock pressure, P_{sh}. A critical component of the model implementation is an algorithm to detect the lead shock. In addition to the cell pressure we examine the detected shock pressure. Of interest is how close P_{sh} is to the VN-spike pressure and the amplitude of fluctuations in the detected shock pressure due to propagating the detonation wave on a discretized grid.

2 Numerical results

All figures are for the numerical solution at the end of the simulation. We first show results for the SURF model. When there are notable differences the results for the SURFplus model will be shown.

Profiles of the pointwise error in the pressure as the resolution increases are shown for the SURF simulations in fig. 3. The pointwise error is dominated by smoothing of the kink in the vicinity of the sonic point; dashed red line in the right plots of fig. 3. This leads to a much larger error in the reaction zone than in the Taylor wave. The noise in the Taylor wave from oscillations in the reaction zone are greatly diminished with finer resolution. For all 3 resolutions, a running average over 41 points smooths out the noise.

Overall, the metric based on $\|P - P_e\|/P_{\mathrm{CJ}}$ goes from 3.96e-4 to 1.42e-4 to 6.62e-5 for cell size of 8, 2, 1 μm. The metric weighs the Taylor wave much more heavily than the reaction zone due to its larger width; factor of about 200 at $t = 10\,\mu$s, see fig. 1. However, the pointwise error is much larger for the reaction zone and it does noticeably contribute to the metric. We note that at later times the metric would be even more heavily weighed to the Taylor wave relative to the ZND reaction zone profile since the width of the Taylor wave increases with time while the reaction zone width is fixed.

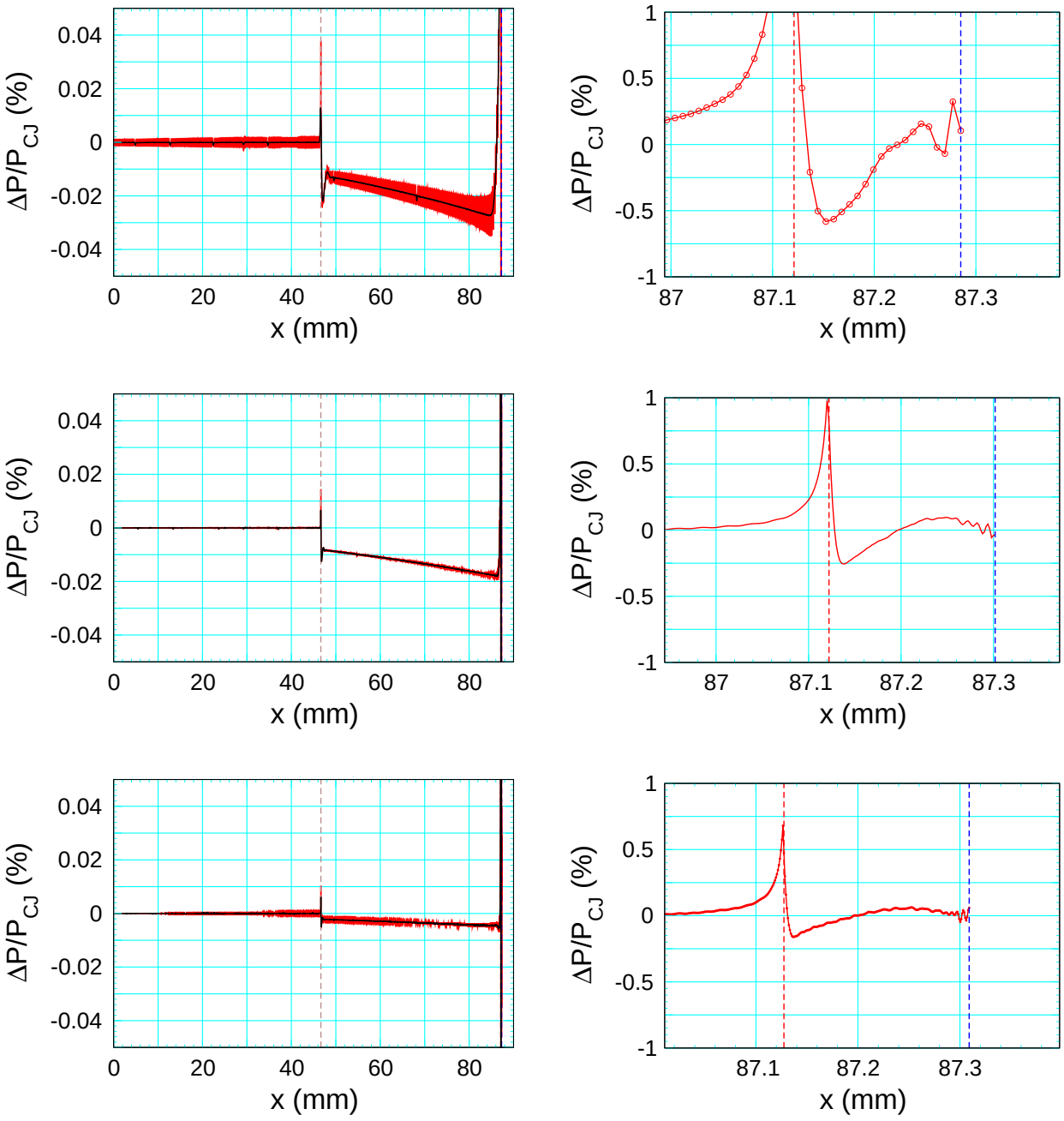

Figure 3: Pointwise error in pressure profiles for the SURF model. Scale on left plots emphasis Taylor wave and on right plots the reaction zone. Top to bottom plots are for cell sizes of 8, 2, 1 μm. On left plots vertical dashed brown line indicates the tail of the Taylor wave, and the black curve is running average over 41 points. On the right plots the vertical dashed blue and red lines indicates the start and end of the reaction zone.

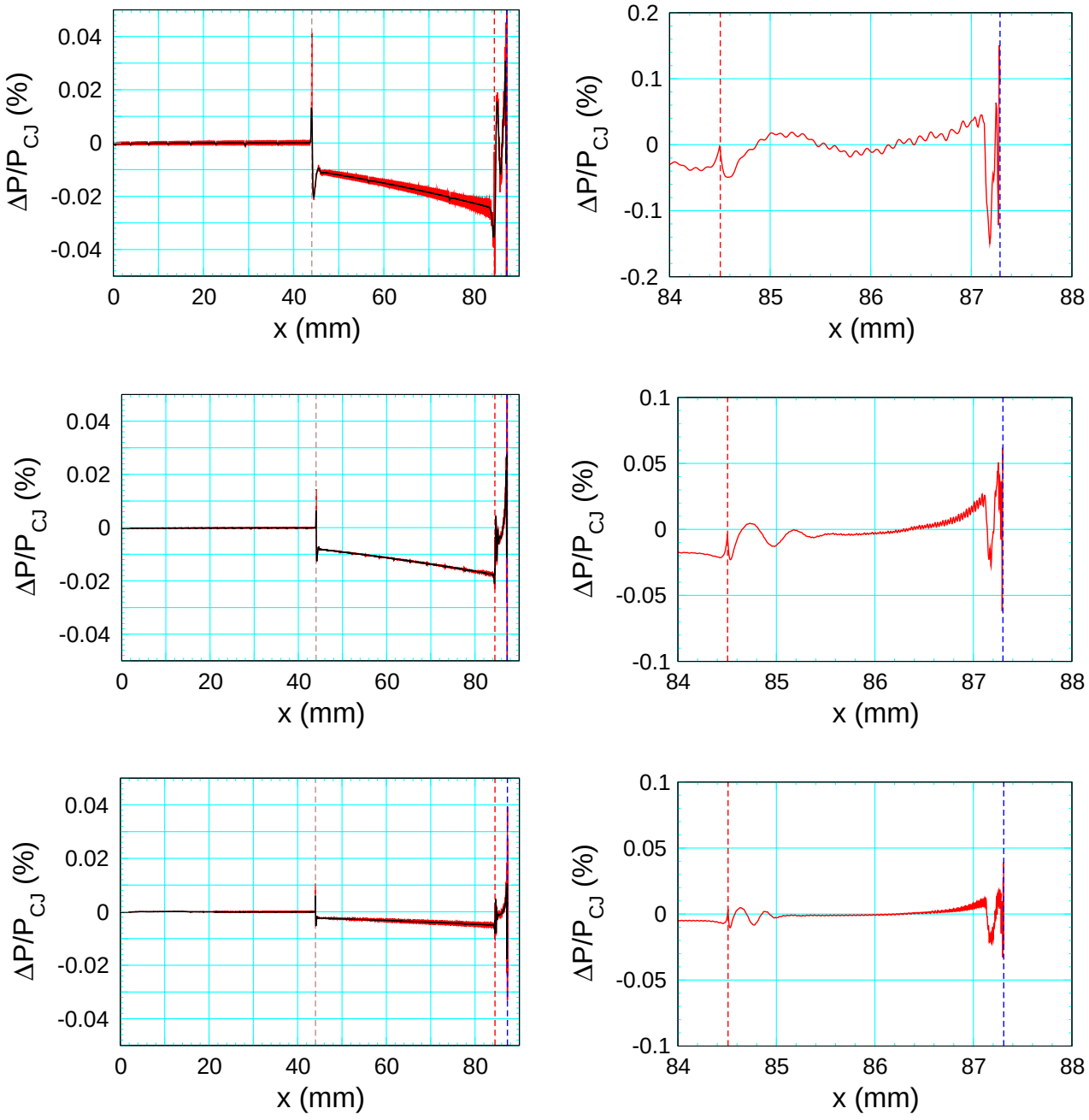

Figure 4: Pointwise error in pressure profiles for the SURFplus model. Scale on left plots emphasis Taylor wave and on right plots the reaction zone. Top to bottom plots are for cell sizes of 8, 2, 1 μm. On left plots vertical dashed brown line indicates the tail of the Taylor wave, and the black curve is running average over 41 points. On the right plots the vertical dashed blue and red lines indicates the start and end of the reaction zone.

The pointwise error in the pressure profiles for the SURFplus model are shown in fig. 4. The error in the reaction zone is smaller for SURFplus due to the smaller magnitude of the kink at the end of the reaction zone. The error in the Taylor wave is about the same as for the SURF model. The overall metric is 1.3e-4, 8.9e-5, 2.6e-5 for cell sizes of 8, 2, 1 μm, respectively. These are slightly smaller than for the SURF simulations.

Profiles of the pressure and reaction progress variable for the SURF model are shown in fig. 5. The numerical shock front can be associated with the peak pressure. With finer resolution, the numerical shock width is thinner. This results in less reaction within the shock rise (5.0, 0.57, 0.27 % for cell sizes of 8, 2, 1 μm respectively), and as we'll see in the next figure a higher shock pressure closer to the exact VN-spike pressure. Also, the pressure kink at the sonic point is sharper (less rounding) as the resolution increases. This reduces the pointwise error in the vicinity of the sonic point as seen in the right plots of fig. 3.

The detected shock pressure for the SURF model is shown in fig. 6 over the spatial range corresponding to the reaction zone. We note that the shock pressure grid variable (left plots) is advected and used for the burn rate. The as detected shock pressure (right plot) is on the time step the lead shock is detected for a given cell, and is not advected. Since numerical advection is diffusive, the shock pressure grid variable is smoothed out behind the shock front, whereas the detected shock pressure has a short wave length oscillation. We note that the same running average (over 41 points) that smooths out the pointwise pressure error in fig. 3 also smooths out the detected shock pressure. Very likely the fluctuations in the detected shock pressure are the source of the noise observed in the pressure profile behind the detonation wave. The smoothed shock pressures of 41.708, 41.878 and 4.897 for cell sizes of 8, 2, 1 μm, respectively, are approaching the VN-spike pressure of 41.905 GPa.

With finer resolution, the lead shock pressure is closer to the exact VN-spike pressure. We also note that the variation of shock pressure is largest for the cells in the neighborhood of the shock front. With more points in the reaction zone, the variation of the shock pressure and hence the burn rate is localized to a smaller neighborhood of the shock front. This reduces the amplitude of the oscillations within the reaction zone, and consequently the magnitude of the acoustic noise transmitted along the left characteristic to the Taylor wave; as seen in left plots of fig. 3.

Profiles in the neighborhood of the sonic point for the SURF model are shown in fig. 7. With finer resolution the sonic point moves closer to the end of the reaction zone. For all resolutions the CJ pressure occurs between the sonic point and the end of the reaction, and closer to the sonic point. The discrepancy between the end of the reaction zone and the sonic point is due to the smoothing of the kink at the sonic point, which also gives rise to the large pointwise error seen in the right plots of fig. 3. The variation in the position of the end of the reaction zone is

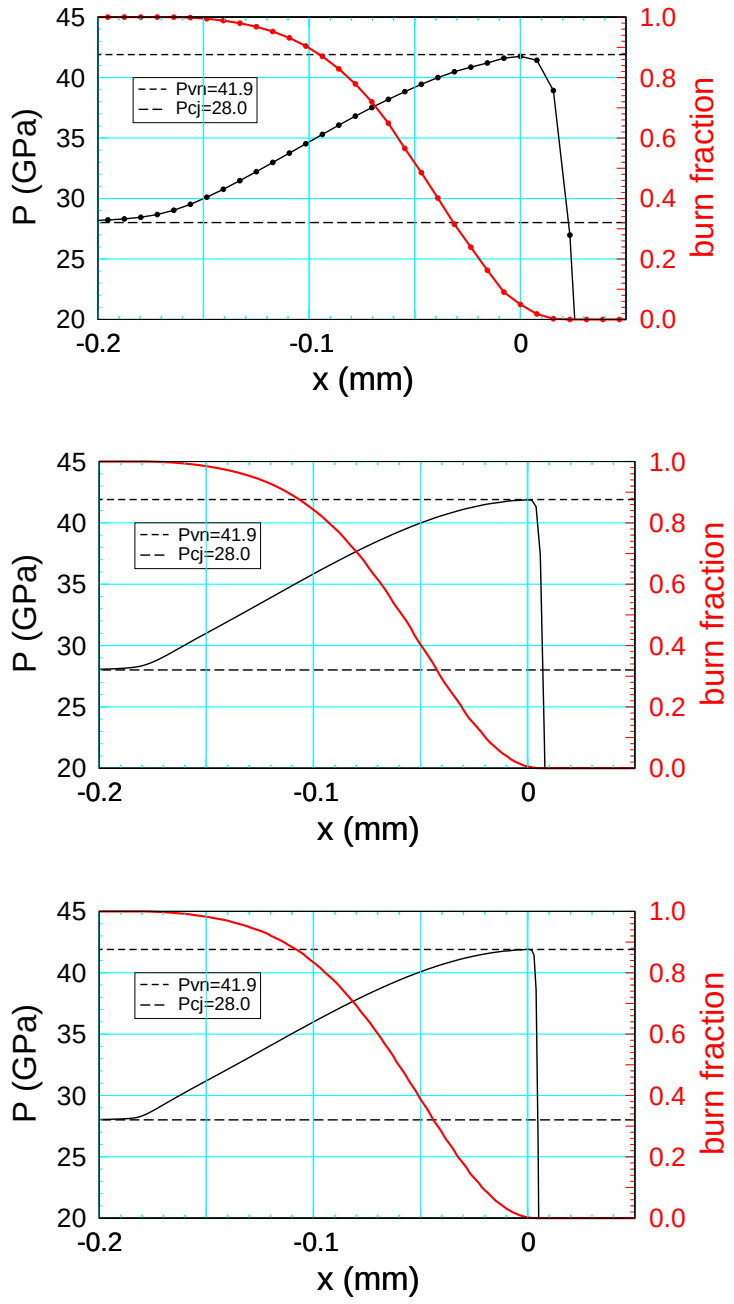

Figure 5: Profile of pressure and reaction progress variable for the SURF model. Short and long dashed lines correspond to the VN-spike and CJ pressures, respectively. Top to bottom plots are for cell sizes of 8, 2, 1 μm. The spatial distance is relative to the numerical shock front; *i.e.*, point of maximum pressure.

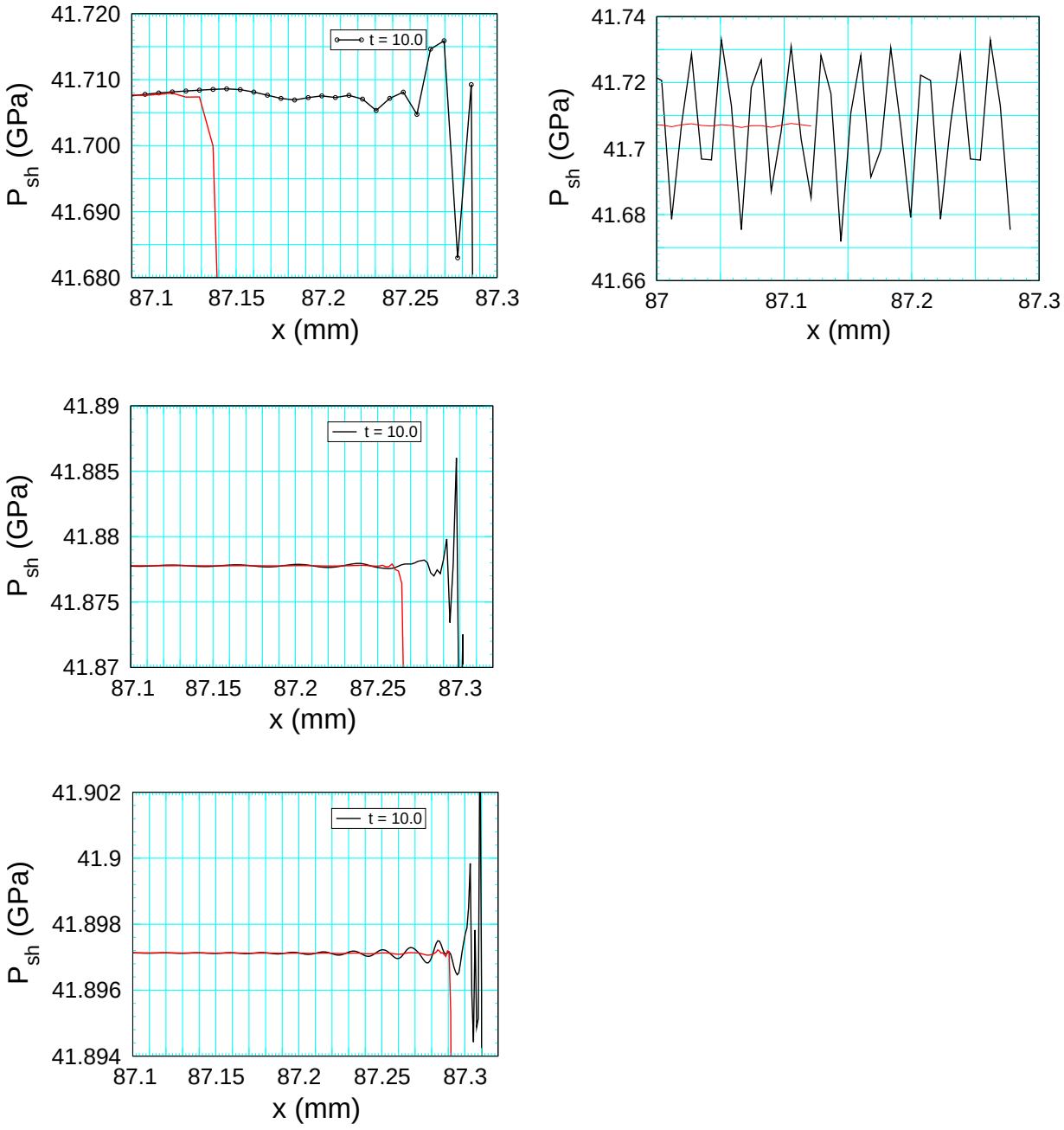

Figure 6: Detected shock pressure for the SURF model over spatial range corresponding to the reaction zone. Left plots are the shock pressure grid variable at $t = 10\,\mu$s. Right plot is the cell shock pressure on the time step the shock is detected. Red line is running average over 41 points. Top to bottom plots are for cell sizes of 8, 2, 1 μm. Note that range of the pressure scales decreases with the cell size, and that the exact VN-spike pressure is 41.905 GPa .

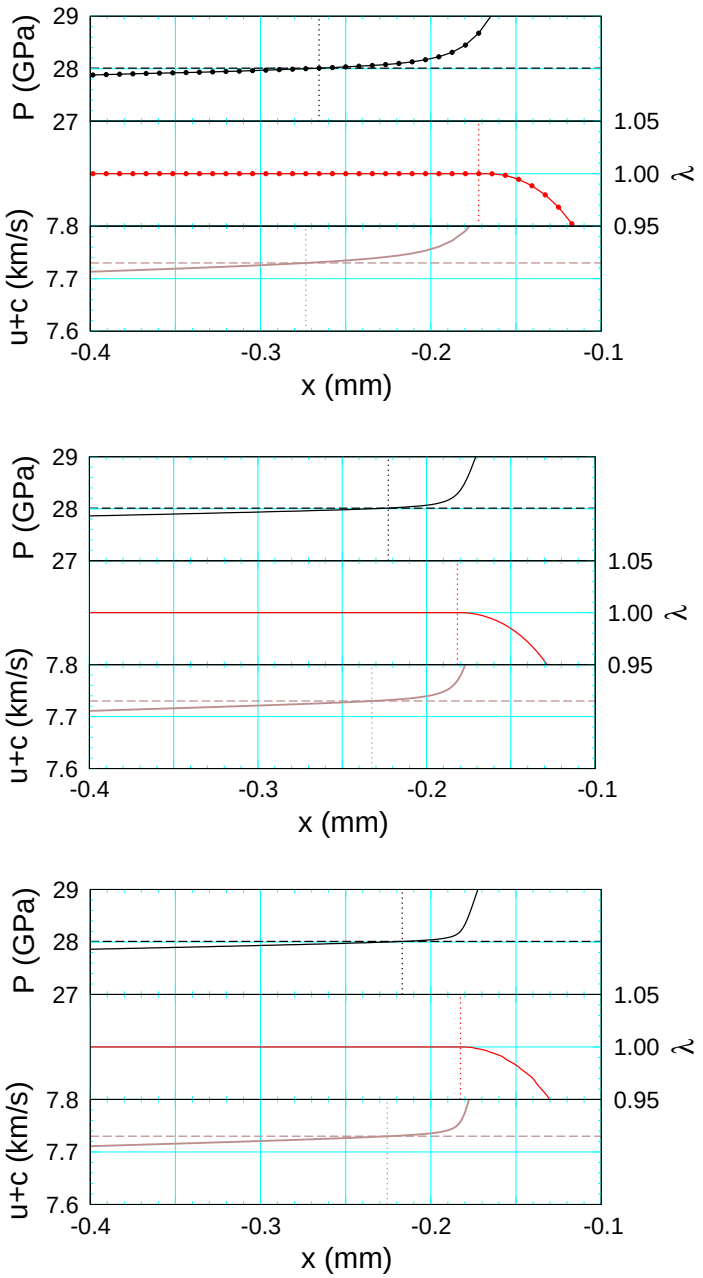

Figure 7: Profiles of pressure, reaction progress variable (λ) and characteristic speed ($u + c$) in the neighborhood of the sonic point for the SURF model. Spatial position is relative to the numerical shock front (taken as the maximum shock pressure). Dashed black line is CJ pressure, and dashed brown line is detonation speed. Dotted lines correspond to the spatial position of CJ pressure ($P = P_{\mathrm{CJ}}$), sonic point ($D = u + c$) and end of reaction zone (largest x with $\lambda = 1$). Top to bottom plots are for cell sizes of 8, 2, 1 μm.

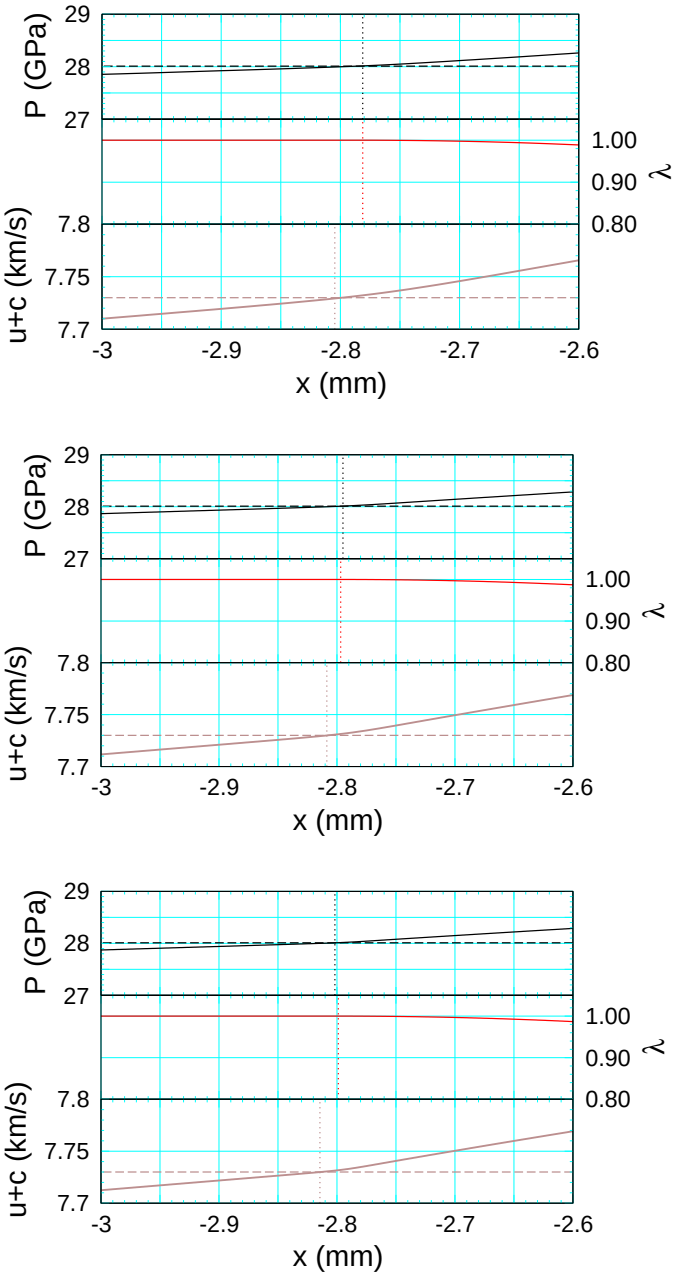

Figure 8: Profiles of pressure, reaction progress variable (λ) and characteristic speed ($u + c$) in the neighborhood of the sonic point for the SURFplus model. Spatial position is relative to the numerical shock front (taken as the maximum shock pressure). Dashed black line is CJ pressure, and dashed brown line is detonation speed. Dotted lines correspond to the spatial position of CJ pressure ($P = P_{\mathrm{CJ}}$), sonic point ($D = u + c$) and end of reaction zone (largest x with $\lambda = 1$). Top to bottom plots are for cell sizes of 8, 2, 1 μm.

due to measuring the spatial position relative to the numerical shock front (peak pressure) and the shock width (as seen in fig. 5).

The sonic point plots for the SURFplus model are shown in fig. 8. The sonic point is closer to end of reaction zone than for the SURF model. Again this is due to the samller magnitude of the kink, which reduces the smoothing of the pressure profile in the neighborhood of the sonic point.

3 Summary

The issue with obtaining an accurate solution for an underdriven (or unsupported) detonation wave is the very narrow reaction zone width compared to the distance that the detonation wave travels. With finer resolution, the numerical solution utilizing the `xRage` code with the SURF and SURFplus models for PBX 9502 improves in several respects:

1. The metric for the overall error in the pressure based on the L_2 norm decreases roughly linearly as the cell size is decreased from 8 to 2 to 1 μm. Due to the disparity in the length scales for the ZND reaction zone and the Taylor wave, the L_2 norm is heavily weighted to the Taylor wave.

2. The pointwise pressure error is dominated by the smearing of the pressure kink in the vicinity of the sonic point, which occurs at the end of the reaction zone. Consequently, the error in the reaction zone is significantly larger than the error in the Taylor wave. The kink is smaller for the SURFplus model due to the longer reaction zone width from the second slow rate. Hence, the resulting error in the reaction zone is smaller.

3. As the cell size decreases, the numerical shock width decreases, and the amount of reaction in the shock profile decreases. In addition, the lead shock pressure gets closer to the VN-spike pressure. With a cell size of 1 μ m, the numerical shock pressure differs from the exact value by 0.007 GPa out of 41.9 GPa; or $\Delta P/P_s$ of 1.7e-4. This is important for the SURF model since the burn rate is a function of the lead shock pressure.

4. The grid variable for the shock pressure is smoothed out by numerical advection. Consequently, variations in the shock pressure profile occur mostly in the neighborhood of the shock front. With finer resolution, the variations are localized to a smaller spatial region. This reduces the amplitude of acoustic noise generated within the reaction zone and then propagated along the left characteristic into the Taylor wave.

5. Due to the smearing of the pressure kink, the sonic point and the CJ pressure occur after the end of the reaction. The discrepancy decreases as the cell size is decreased.

References

W. Fickett and W. C. Davis. *Detonation*. Univ. of Calif. Press, 1979. 2

R. Menikoff. Verification test of the SURF and SURFplus models in xRage. Technical Report LA-UR-16-23636, Los Alamos National Lab., 2016. URL http://www.osti.gov/scitech/servlets/purl/1254247. 2

R. Menikoff and M. S. Shaw. Reactive burn models and ignition & growth concept. *EPJ Web of Conferences*, 10, 2010. doi: 10.1051/epjconf/20101000003. URL http://www.epj-conferences.org/articles/epjconf/pdf/2010/09/epjconf_nmh2010_00003.pdf. 2

R. Menikoff and M. S. Shaw. The SURF model and the curvature effect for PBX 9502. *Combustion Theory And Modelling*, pages 1140–1169, 2012. doi: 10.1080/13647830.2012.713994. 2

M. S. Shaw and R. Menikoff. Reactive burn model for shock initiation in a PBX: Scaling and separability based on the hot spot concept. In *Fourteenth Symposium (International) on Detonation*, 2010. 2